J. Fluid Mech. (2022), *vol*. 934, R3, doi:10.1017/jfm.2021.1148

Nonlinear multiphase flow in hydrophobic porous media

Yihuai Zhang[1],†, **Branko Bijeljic**[1] **and Martin J. Blunt**[1]

[1]Department of Earth Science and Engineering, Imperial College London, London SW7 2BP, UK

(Received 23 August 2021; revised 4 December 2021; accepted 20 December 2021)

Multiphase flow in porous materials is conventionally described by an empirical extension to Darcy's law, which assumes that the pressure gradient is proportional to the flow rate. Through a series of two-phase flow experiments, we demonstrate that even when capillary forces are dominant at the pore scale, there is a nonlinear intermittent flow regime with a power-law dependence between pressure gradient and flow rate. Energy balance is used to predict accurately the start of the intermittent regime in hydrophobic porous media. The pore-scale explanation of the behaviour based on the periodic filling of critical flow pathways is confirmed through 3D micron-resolution X-ray imaging.

Key words: multiphase flow

1. Introduction

Multiphase flow in porous media occurs in a wide variety of natural and engineered settings, including carbon geosequestration, geoenergy resources recovery, subsurface contaminant control, drug delivery and flow in fuel cells (Berg *et al.* 2013; Pak *et al.* 2015; Reynolds & Krevor 2015; Blunt 2017; Zhao *et al.* 2018; Iglauer *et al.* 2019; Zhang *et al.* 2019; Zhao *et al.* 2019; Gjennestad, Winkler & Hansen 2020; Gao *et al.* 2021; Zhang *et al.* 2021). For the last 85 years, multiphase flow has been quantified assuming that each fluid phase has its own pathway and the flow rate has a linear relationship with pressure gradient, governed by an empirical extension of Darcy's law (Muskat & Meres 1936; Muskat 1938; Blunt 2017),

$$q_i = -\frac{k_{ri}K}{\mu_i}(\nabla P_i - \rho_i g), \tag{1.1}$$

where q_i is the Darcy flux, defined as the volume of phase i flowing per unit area per unit time, K is the absolute permeability of the sample, k_{ri} is the relative permeability, μ_i is the

† Email address for correspondence: yihuai.zhang@imperial.ac.uk

viscosity, ∇P_i is the pressure gradient for phase i and $\rho_i g$ is the contribution of gravity, which is ignored in this study.

The capillary number Ca is defined as $Ca = \mu q_t/\sigma$, where μ is the average viscosity of the two fluids, q_t is the total Darcy flux of the two phases and σ is the interfacial tension. It is well known that Ca has a linear relationship with pressure gradient ∇P at low flow rate, $\nabla P \sim Ca$ (Blunt 2017; Gao *et al.* 2020; Zhang *et al.* 2021).

Recent research has shown that there is nonlinear flow even at low capillary numbers where the capillary force is still dominant at the pore scale (Rassi, Codd & Seymour 2011; Sinha & Hansen 2012; Armstrong & Berg 2013; Rücker *et al.* 2015; Gao *et al.* 2020). We observe a so-called intermittent regime with $\nabla P \sim Ca^a$, $1 > a > 0$: the pressure gradient has a power-law relation with flow rate. At the pore scale, some regions of the void space, which provide additional connectivity, are intermittently occupied by both phases, as confirmed through high-resolution X-ray imaging and confocal microscopy (Datta, Dupin & Weitz 2014; Gao *et al.* 2017; Reynolds *et al.* 2017; Spurin *et al.* 2019*a*, *b*; Gao *et al.* 2020). This phenomenon is associated with non-thermal and non-periodic fluctuations in pressure and fluid occupancy representing a nonlinear disordered dynamics (Rücker *et al.* 2021). Tallakstad *et al.* (2009) was the first to observe this behaviour and suggested that $a \approx 0.5$ from two-phase flow experiments in a quasi-two-dimensional porous medium. Sinha *et al.* (2017) also proposed $a = 0.5$ through an analysis of experiments and simulations. Gao *et al.* (2020) found a threshold capillary number for the onset of intermittency Ca^i of approximately 10^{-5} in two-phase steady-state flow tests on a water-wet (hydrophilic) sandstone sample with a water fractional flow (ratio of the volumetric flow rate of water to the total flow rate of oil and water) $f_w = 0.5$, where the exponent a was approximately 0.6. Recently, Zhang *et al.* (2021) quantified the onset of intermittency as a function of fractional flow for fluids with different viscosity ratio and different rock types. To date, however, only two studies have investigated non-hydrophilic media, which have suggested that there may be more intermittency under these conditions (Zou *et al.* 2018; Rücker *et al.* 2019).

In many natural and engineered settings, including soils containing organic material, gas diffusion layers in fuel cells, surgical masks and rock that has been in contact with hydrocarbons, the solid surfaces of the porous material are not uniformly hydrophilic. It is more common to encounter a range of local contact angles, both above and below 90°, representing a mixed-wet state (AlRatrout, Blunt & Bijeljic 2018). However, there have been no quantitative studies of the onset of intermittency under these conditions.

In this paper, we conduct 174 steady-state immiscible two-phase flow experiments through an altered-wettability Bentheimer sandstone sample with different water fractional flows ($f_w = 0.2$, 0.4, 0.5, 0.6, 0.7 and 0.8), where the capillary number varies from $\sim 10^{-7}$ to $\sim 10^{-4}$ during a waterflood displacement. We label the sample 'hydrophobic', although the pore surfaces locally have a range of contact angle with both hydrophilic and hydrophobic regions (Lin *et al.* 2019). We also performed high-resolution pore-scale imaging on a replicate sample for 14 flow rates and fractional flows covering both the linear and intermittent flow regimes. We use energy balance to predict accurately the boundary of the onset of intermittency, which is consistent with our experimental results and *in situ* pore-scale X-ray images.

2. Materials and methods

We studied two Bentheimer sandstone samples (samples A and B, drilled from the same block). First, the samples were completely saturated with brine. The absolute

permeability of the samples was measured during single-phase brine flow to be $K = 1.85\ (\pm 0.02) \times 10^{-12}$ m^2 (Zhang *et al.* 2021). Then, crude oil from the Middle East was injected and the samples were left in the crude oil for two months at 80 °C and 3 MPa pressure. Direct contact of the crude oil with parts of the solid surface altered the wettability from water-wet to a more mixed-wet to oil-wet state, which we will call, for convenience, 'hydrophobic' (Lin *et al.* 2019, 2021). Decane was injected at 3 ml min^{-1} for 60 min to replace the crude oil. Sample A (5.97 mm diameter and 27.88 mm length) was mounted in a specially designed flooding system (Gao *et al.* 2017, 2020). The water (brine) phase was 15 wt% KI (potassium iodide) brine, and the oil phase was *n*-decane, both injected by high-precision ISCO pumps through a dual injection port (Zhang *et al.* 2021). The measured viscosity of the brine was 0.821 mPa s, the *n*-decane viscosity was 0.838 mPa s (PubChem, Open Chemistry database), while the interfacial tension was measured to be $\sigma = 47$ mN m^{-1}.

During the experiments, a high-precision pressure transducer (Keller PD-33) recorded the pressure difference between the inlet and outlet of the sample. Similar to the experimental protocol in Zhang *et al.* (2021), we started the two-phase flow experiment from a low water fractional flow and low flow rate: f_w of 0.2 at 0.02 ml min^{-1} total flow rate ($Ca = 2.1 \times 10^{-7}$). The pressure gradient was recorded after 12 h when it stabilized, and then the flow rate increased from low to high and the pressure gradients at steady state were recorded. A total of 29 flow rates were considered for each f_w: the highest flow rate was 4.5 ml min^{-1} ($Ca = 4.8 \times 10^{-5}$). Note that the time for the pressure gradient to stabilize depended on the flow rate: it took up to 12 h for the low flow rate (0.02 ml min^{-1}), while as little as 5 min for the highest rates (greater than 3 ml min^{-1}). The *n*-decane was injected at 3 ml min^{-1} for 30 min again to return to the initial saturation after each sequence of experiments at the same fractional flow. We repeated this injection sequence for other fractional flows: 0.4, 0.5, 0.6, 0.7, and 0.8; in total 174 flow experiments were conducted.

For sample B (6.15 mm diameter and 50.13 mm length), we have followed the same experimental protocol as for sample A but replaced the water phase with 30 wt% KI brine for a better X-ray contrast; the viscosity of the brine was measured as 0.819 mPa s (Gao *et al.* 2019). The flooding system was placed in a Zeiss XRM-510 X-ray microscope for high-resolution *in situ* imaging (Zhang *et al.* 2016; Lebedev *et al.* 2017; Gao *et al.* 2019; Lin *et al.* 2019). The scan setting was 3.58 μm voxel size, 0.5 s exposure time, 75 kV X-ray energy and 1601 projections with a flat panel detector. The scan time was around 1 h. We selected and repeated 14 test points: 0.1, 0.2 and 0.8 ml min^{-1} flow rates for $f_w = 0.2$; 0.1, 0.2, 0.8 and 1.25 ml min^{-1} flow rates for $f_w = 0.5$; 0.1, 0.2, 0.8 and 1.25 ml min^{-1} flow rates for $f_w = 0.7$; and 0.1, 0.2 and 0.8 ml min^{-1} flow rates for $f_w = 0.8$.

3. Results

The results, for all water fractional flows f_w, clearly show a transition from a linear $a = 1$ to a nonlinear regime $a < 1$ when the capillary number increases (figure 1). We found that the exponent a and threshold capillary number Ca^i are both functions of the fractional flow (see table 1). The lowest value $a = 0.50 \pm 0.01$ occurs when $f_w = 0.4$, indicating the strongest intermittency, defined as the deviation from a linear Darcy law; $f_w = 0.8$ had the highest exponent $a = 0.58 \pm 0.01$, indicating weaker intermittency. The range of a is smaller when compared with similar experiments on a water-wet sample, where a varied

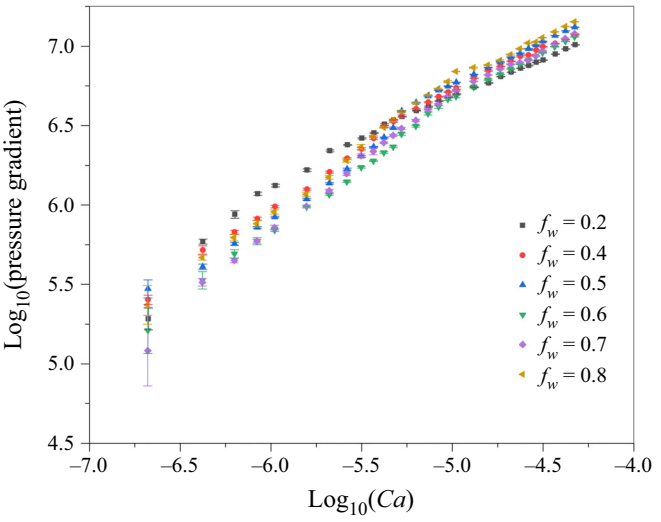

Figure 1. Summary of the measured pressure gradient ∇P as a function of capillary number Ca, for different water fractional flows f_w: 0.2, 0.4, 0.5, 0.6, 0.7 and 0.8.

Fractional flow (f_w)	a ($Ca < Ca^i$)	Ca^i	Ca^i_1	Ca^i_2	a ($Ca > Ca^i$)
0.2	1	$\sim 10^{-5.7}$	$\sim 10^{-5.8}$	$\sim 10^{-6.4}$	0.55 ± 0.01
0.4	1	$\sim 10^{-5.4}$	$\sim 10^{-5.6}$	$\sim 10^{-5.8}$	0.50 ± 0.01
0.5	1	$\sim 10^{-5.3}$	$\sim 10^{-5.6}$	$\sim 10^{-5.6}$	0.51 ± 0.01
0.6	1	$\sim 10^{-5.2}$	$\sim 10^{-5.6}$	$\sim 10^{-5.4}$	0.56 ± 0.01
0.7	1	$\sim 10^{-5.1}$	$\sim 10^{-5.7}$	$\sim 10^{-5.3}$	0.57 ± 0.01
0.8	1	$\sim 10^{-5.1}$	$\sim 10^{-5.8}$	$\sim 10^{-5.2}$	0.58 ± 0.01

Table 1. Summary of the exponent a for $\nabla P \sim Ca^a$, threshold capillary number Ca^i for the onset of intermittency, and the associated oil-phase capillary number Ca^i_1 and water-phase capillary number Ca^i_2, from figure 1.

from 0.44 to 0.74 (Zhang *et al.* 2021). Moreover, the lower fractional flows have smaller threshold capillary numbers Ca^i for the onset of intermittency: Ca^i increased from $10^{-5.7}$ to $10^{-5.1}$ as the water fractional flow f_w increased from 0.2 to 0.8; this is the opposite trend to the water-wet results.

In the high-resolution images (figure 2), it is evident that large pores are occupied by water, as expected for media that are no longer water-wet (Gao *et al.* 2020). We used an automated method to calculate contact angles directly on the images at the three-phase (oil–water–solid) contact line (AlRatrout *et al.* 2017) for $f_w = 0.5$, 0.1 ml min^{-1} injection rate, $Ca = 10^{-6}$. The average contact angle is 103°, with a standard deviation of 22°, representing, on average, a hydrophobic medium (mixed-wet or oil-wet) (Lin *et al.* 2019). However, the sample is not uniformly hydrophobic: locally, there are contact angles both less than 90° (hydrophilic) and greater than 90° (hydrophobic).

At the pore scale, it has been shown, in uniformly water-wet systems, that the nonlinear flow behaviour is caused by intermittent filling of regions of the pore space alternately by both phases; the oil and water no longer travel through fixed flow pathways and become quasi steady-state (Gao *et al.* 2020). We use our images to quantify regions of the pore

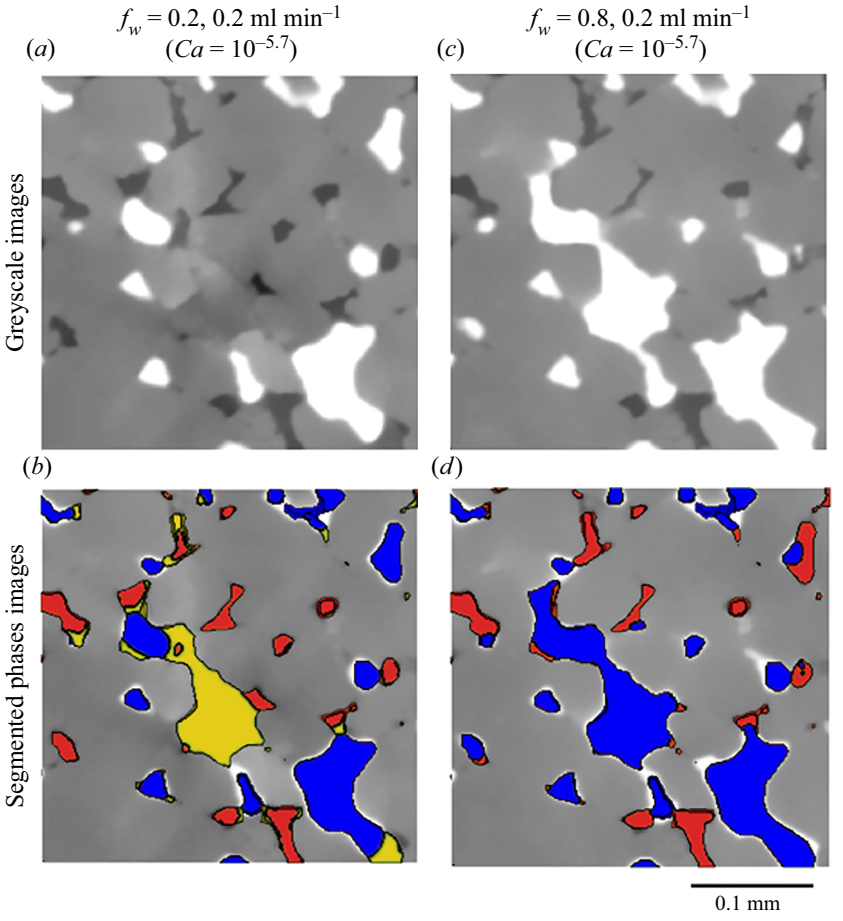

Figure 2. Example two-dimensional cross-sections of three-dimensional images showing phase configurations in the same area of the rock sample at the same flow rate (0.2 ml min^{-1}) but different water fractional flows: $f_w = 0.2$ (*a*,*b*) and 0.8 (*c*,*d*). The capillary number is $10^{-5.7}$. (*a*) and (*c*) are greyscale images, and (*b*) and (*d*) are segmented images, where blue is water, red is oil and yellow represents intermittent regions that were periodically occupied by both oil and water during the 1 h scan time.

space that are always occupied by oil during the scan time of 1 h, always occupied by water, and intermittent regions, identified by intermediate greyscale values, which are occupied by both oil and water during the scan time. As an example, figure 2 shows that there is more intermittency for the lower water fractional flows, consistent with the threshold capillary numbers and exponents listed in table 1. figure 3 demonstrates how the degree of intermittency increases with flow rate. In the Darcy regime, the volume of any intermittent regions is negligible and the two phases flow through fixed flow pathways. In the intermittent regime, a significant fraction of the pore space is periodically occupied by both phases, facilitating flow; more pathways open up as the capillary number increases, leading to a nonlinear relationship between flow rate and pressure gradient.

4. Quantification of the transition from linear to intermittent flow

We now quantify the onset of intermittency using an energy balance argument. We generalize our previous work Zhang *et al.* (2021) by identifying oil as the wetting phase

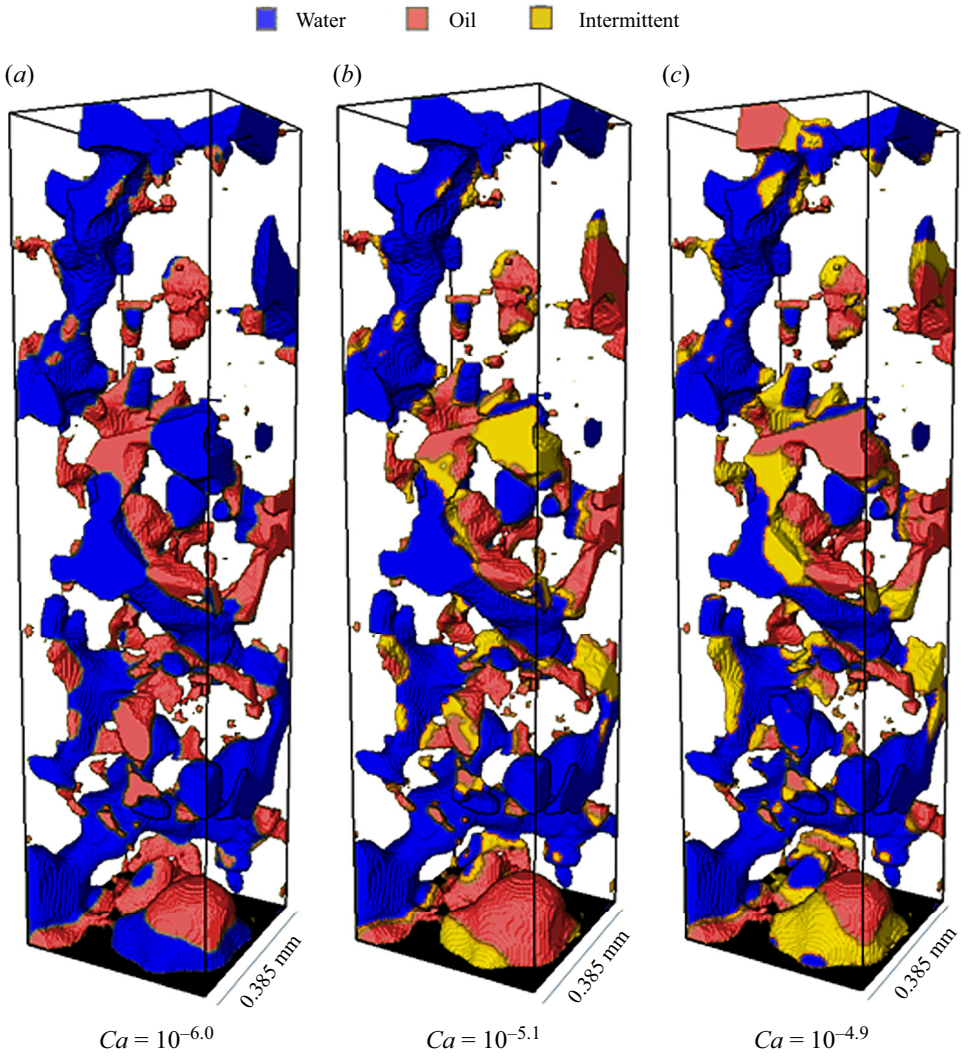

Figure 3. Three-dimensional views of the segmented phases on a 100 × 100 × 400 voxels sub-volume of the full image for $f_w = 0.7$ and $Ca = 10^{-6.0}$, $10^{-5.1}$ and $10^{-4.9}$. Water is blue, oil is red and intermittent regions are shown in yellow.

(which we label phase 1) and water as non-wetting (which we label phase 2). We hypothesize that intermittency first occurs when the work done due to fluid injection over a characteristic pore scale l is sufficient to create a fluid meniscus. Note that this is not the same as equating the pressure drop across a pore to the capillary pressure, which occurs at higher flow rates. We define l as a characteristic distance between pores. The average pore volume associated with a pore is thus ϕl^3, where ϕ is the porosity. The change in pressure P over a distance l is equal to $-l\nabla P$, where ∇P is the pressure gradient. The mechanical work of fluid injection, $P\nabla V$, can be written as $-\phi l^4 \nabla P$. The energy to create an interface in a pore of typical radius r is σr^2, which, at the onset of intermittency, we assume is equal to $-\phi l^4 \nabla P$. We ignore the change in surface energy due to changes in the fluid–solid interfacial areas.

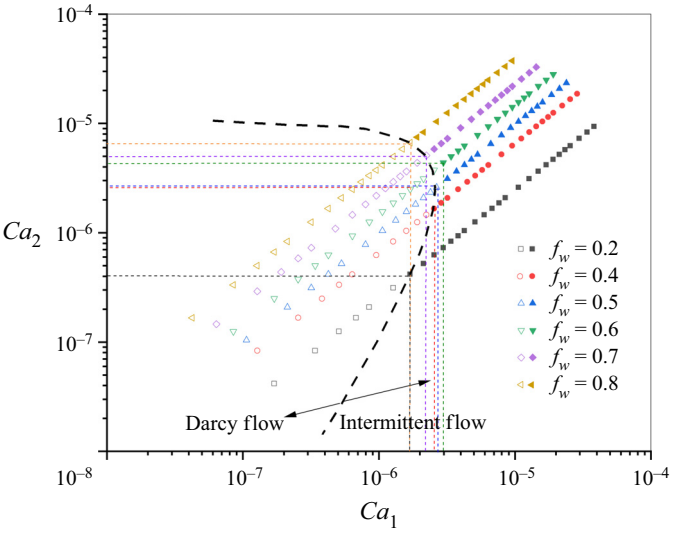

Figure 4. The phase diagram showing linear flow (empty symbols) and nonlinear flow (filled symbols) for sample A as a function of oil capillary number Ca_1^i and water capillary number Ca_2^i. The black dashed line is the predicted transition from Darcy to intermittent flow using (4.2) and (4.3).

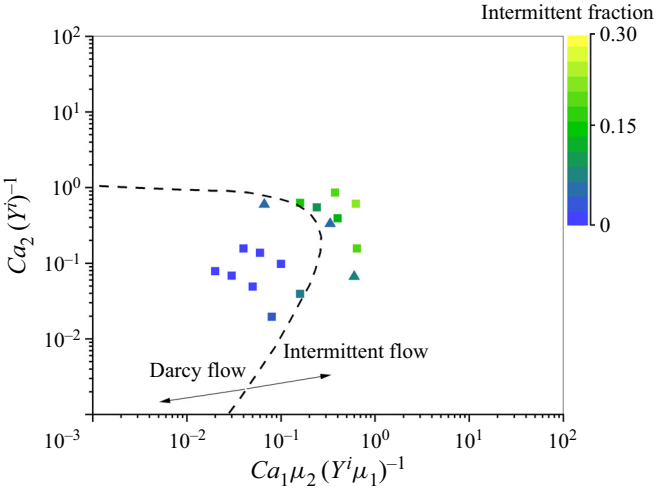

Figure 5. The replotted phase diagram showing the fraction of the pore space that has intermittent occupancy; the squares are for sample B, and the triangles are data from the literature (Zou *et al.* 2018). The dashed line is the predicted transition from Darcy to intermittent flow using (4.2) and (4.3).

To estimate the pressure gradient, we assume Darcy-like flow on average with a total flow rate q_t^i and a limiting mobility f_w/μ_1, which represents flow of the wetting phase (1, oil) into and out of regions of the pore space filled with the non-wetting phase (2, water) with an effective relative permeability, at least in the viscous-flow limit of f_w. Hence from (1.1) we estimate $\nabla P \approx -\mu_1 q_t^i / K f_w$. We then expect the onset of intermittency when

$$\sigma r^2 = \frac{\mu_1 q_t^i \phi l^4}{K f_w}. \tag{4.1}$$

This can be rearranged to write the threshold water (non-wetting) phase capillary number $Ca_2^i = \mu_2 f_w q_t^i/\sigma$ and oil (wetting) phase capillary number $Ca_1^i = \mu_1(1-f_w)q_t^i/\sigma$ as

$$Ca_2^i = Y^i(f_w)^2 \tag{4.2}$$

and

$$Ca_1^i = Y^i f_w(1-f_w)\frac{\mu_1}{\mu_2}, \tag{4.3}$$

and the dimensionless number Y^i is defined by

$$Y^i = \frac{\mu_2}{\mu_1}\frac{Kr^2}{\phi l^4}. \tag{4.4}$$

For Bentheimer sandstone, the mean pore radius r is 24 μm (Blunt 2017) and l has a value of approximately 150 μm (Gao *et al.* 2020), which is the mean pore-to-pore distance obtained from pore-network analysis (Raeini, Bijeljic & Blunt 2017). Then we calculate Y^i to be $\approx 10^{-5}$.

In figure 4, our results for sample A (table 1) are plotted on a phase diagram as a function of Ca_1 and Ca_2 (Datta *et al.* 2014). Equations (4.2) and (4.3) accurately predict the onset of intermittency for all fractional flows.

Furthermore, we quantify the fraction of the pore space that is intermittently occupied based on the pore-scale images for sample B (figure 5). In the Darcy regime, it has zero intermittent phase or a small amount of intermittent occupancy that is insufficient to perturb the linear Darcy law (Gao *et al.* 2020). Once nonlinear behaviour emerges, the fraction of the pore space periodically occupied by both phases increases up to 28 % in the cases studied. In figure 5, we also show a good agreement between our theory and previously published work for mixed-wet Bentheimer sandstone from Zou *et al.* (2018), with a different viscosity ratio (the oil–water viscosity ratio was 1.46), where the three experiments are all in the predicted intermittent regime or near the threshold line. It should be noted that in previous work we showed that the energy balance theory also accurately predicted the onset of intermittency for a wide range of data in the literature on water-wet samples for different rock types and viscosity ratios (Zhang *et al.* 2021).

5. Conclusions

We have measured the pressure gradient and imaged the nonlinear pore-scale dynamics as a function of capillary number for different water fractional flows on hydrophobic porous media with a wide range of local contact angle during steady-state immiscible two-phase displacement. The Darcy flow regime and the transition to intermittent flow regime have been observed. Using energy balance, we have proposed the threshold line for the onset of intermittent flow, (4.2) and (4.3), which accurately matches the experimental results and is consistent with the pore-scale images. The work provides a quantification of nonlinear flow that is likely to be encountered in many processes, including carbon dioxide storage, subsurface gas production, in porous fibrous layers within fuel cells, microfluidics devices used in drug delivery, and catalysis, which involve multiphase fluid flow in porous materials.

Acknowledgements. We are grateful to Dr S. Berg for many useful discussions on this work.

Funding. We gratefully acknowledge funding from the Shell Digital Rocks programme at Imperial College London.

Declaration of interests. The authors report no conflict of interest.

Author ORCIDs.
Yihuai Zhang https://orcid.org/0000-0001-5471-3450.

References

ALRATROUT, A., BLUNT, M.J. & BIJELJIC, B. 2018 Wettability in complex porous materials, the mixed-wet state, and its relationship to surface roughness. *Proc. Natl Acad. Sci. USA* **115** (36), 8901–8906.

ALRATROUT, A., RAEINI, A.Q., BIJELJIC, B. & BLUNT, M.J. 2017 Automatic measurement of contact angle in pore-space images. *Adv. Water Resour.* **109**, 158–169.

ARMSTRONG, R.T. & BERG, S. 2013 Interfacial velocities and capillary pressure gradients during Haines jumps. *Phys. Rev.* E **88** (4), 043010.

BERG, S., *et al.* 2013 Real-time 3D imaging of Haines jumps in porous media flow. *Proc. Natl Acad. Sci. USA* **110** (10), 3755–3759.

BLUNT, M.J. 2017 *Multiphase Flow in Permeable Media: A Pore-Scale Perspective*. Cambridge University Press.

DATTA, S.S., DUPIN, J.-B. & WEITZ, D.A. 2014 Fluid breakup during simultaneous two-phase flow through a three-dimensional porous medium. *Phys. Fluids* **26** (6), 062004.

GAO, Y., LIN, Q., BIJELJIC, B. & BLUNT, M.J. 2017 X-ray microtomography of intermittency in multiphase flow at steady state using a differential imaging method. *Water Resour. Res.* **53** (12), 10274–10292.

GAO, Y., LIN, Q., BIJELJIC, B. & BLUNT, M.J. 2020 Pore-scale dynamics and the multiphase Darcy law. *Phys. Rev. Fluids* **5** (1), 013801.

GAO, Y., RAEINI, A.Q., BLUNT, M.J. & BIJELJIC, B. 2019 Pore occupancy, relative permeability and flow intermittency measurements using X-ray micro-tomography in a complex carbonate. *Adv. Water Resour.* **129**, 56–69.

GAO, Y., RAEINI, A.Q., BLUNT, M.J. & BIJELJIC, B. 2021 Dynamic fluid configurations in steady-state two-phase flow in Bentheimer sandstone. *Phys. Rev.* E **103** (1), 013110.

GJENNESTAD, M.A., WINKLER, M. & HANSEN, A. 2020 Pore network modeling of the effects of viscosity ratio and pressure gradient on steady-state incompressible two-phase flow in porous media. *Transp. Porous Media* **132** (2), 355–379.

IGLAUER, S., PALUSZNY, A., RAHMAN, T., ZHANG, Y., WÜLLING, W. & LEBEDEV, M. 2019 Residual trapping of CO_2 in an oil-filled, oil-wet sandstone core: results of three-phase pore-scale imaging. *Geophys. Res. Lett.* **46** (20), 11146–11154.

LEBEDEV, M., ZHANG, Y., SARMADIVALEH, M., BARIFCANI, A., AL-KHDHEEAWI, E. & IGLAUER, S. 2017 Carbon geosequestration in limestone: pore-scale dissolution and geomechanical weakening. *Intl J. Greenh. Gas Control* **66**, 106–119.

LIN, Q., BIJELJIC, B., BERG, S., PINI, R., BLUNT, M.J. & KREVOR, S. 2019 Minimal surfaces in porous media: pore-scale imaging of multiphase flow in an altered-wettability Bentheimer sandstone. *Phys. Rev.* E **99** (6), 063105.

LIN, Q., BIJELJIC, B., FOROUGHI, S., BERG, S. & BLUNT, M.J. 2021 Pore-scale imaging of displacement patterns in an altered-wettability carbonate. *Chem. Engng Sci.* **235**, 116464.

MUSKAT, M. 1938 The flow of homogeneous fluids through porous media. *Soil Sci.* **46** (2), 169.

MUSKAT, M. & MERES, M.W. 1936 The flow of heterogeneous fluids through porous media. *Physics* **7** (9), 346–363.

PAK, T., BUTLER, I.B., GEIGER, S., VAN DIJKE, M.I.J. & SORBIE, K.S. 2015 Droplet fragmentation: 3D imaging of a previously unidentified pore-scale process during multiphase flow in porous media. *Proc. Natl Acad. Sci. USA* **112** (7), 1947–1952.

RAEINI, A.Q., BIJELJIC, B. & BLUNT, M.J. 2017 Generalized network modeling: network extraction as a coarse-scale discretization of the void space of porous media. *Phys. Rev.* E **96** (1), 013312.

RASSI, E.M., CODD, S.L. & SEYMOUR, J.D. 2011 Nuclear magnetic resonance characterization of the stationary dynamics of partially saturated media during steady-state infiltration flow. *New J. Phys.* **13** (1), 015007.

REYNOLDS, C.A. & KREVOR, S. 2015 Characterizing flow behavior for gas injection: relative permeability of CO_2-brine and N_2-water in heterogeneous rocks. *Water Resour. Res.* **51** (12), 9464–9489.

REYNOLDS, C.A., MENKE, H., ANDREW, M., BLUNT, M.J. & KREVOR, S. 2017 Dynamic fluid connectivity during steady-state multiphase flow in a sandstone. *Proc. Natl Acad. Sci. USA* **114** (31), 8187–8192.

RÜCKER, M., *et al.* 2015 From connected pathway flow to ganglion dynamics. *Geophys. Res. Lett.* **42** (10), 3888–3894.

RÜCKER, M., *et al.* 2019 The effect of mixed wettability on pore-scale flow regimes based on a flooding experiment in Ketton limestone. *Geophys. Res. Lett.* **46** (6), 3225–3234.

RÜCKER, M., GEORGIADIS, A., ARMSTRONG, R.T., OTT, H., BRUSSEE, N., VAN DER LINDE, H., SIMON, L., ENZMANN, F., KERSTEN, M. & BERG, S. 2021 The origin of non-thermal fluctuations in multiphase flow in porous media. *Front. Water* **3**, 671399.

SINHA, S., BENDER, A.T., DANCZYK, M., KEEPSEAGLE, K., PRATHER, C.A., BRAY, J.M., THRANE, L.W., SEYMOUR, J.D., CODD, S.L. & HANSEN, A. 2017 Effective rheology of two-phase flow in three-dimensional porous media: experiment and simulation. *Transp. Porous Med.* **119** (1), 77–94.

SINHA, S. & HANSEN, A. 2012 Effective rheology of immiscible two-phase flow in porous media. *Europhys. Lett.* **99** (4), 44004.

SPURIN, C., BULTREYS, T., BIJELJIC, B., BLUNT, M.J. & KREVOR, S. 2019*a* Intermittent fluid connectivity during two-phase flow in a heterogeneous carbonate rock. *Phys. Rev.* E **100** (4), 043103.

SPURIN, C., BULTREYS, T., BIJELJIC, B., BLUNT, M.J. & KREVOR, S. 2019*b* Mechanisms controlling fluid breakup and reconnection during two-phase flow in porous media. *Phys. Rev.* E **100** (4), 043115.

TALLAKSTAD, K.T., KNUDSEN, H.A., RAMSTAD, T., LØVOLL, G., MÅLØY, K.J., TOUSSAINT, R. & FLEKKØY, E.G. 2009 Steady-state two-phase flow in porous media: statistics and transport properties. *Phys. Rev. Lett.* **102** (7), 074502.

ZHANG, Y., BIJELJIC, B., GAO, Y., LIN, Q. & BLUNT, M.J. 2021 Quantification of nonlinear multiphase flow in porous media. *Geophys. Res. Lett.* **48** (5), e2020GL090477.

ZHANG, Y., LEBEDEV, M., JING, Y., YU, H. & IGLAUER, S. 2019 In-situ x-ray micro-computed tomography imaging of the microstructural changes in water-bearing medium rank coal by supercritical CO_2 flooding. *Intl J. Coal Geol.* **203**, 28–35.

ZHANG, Y., LEBEDEV, M., SARMADIVALEH, M., BARIFCANI, A. & IGLAUER, S. 2016 Swelling-induced changes in coal microstructure due to supercritical CO_2 injection. *Geophys. Res. Lett.* **43** (17), 9077–9083.

ZHAO, B., *et al.* 2019 Comprehensive comparison of pore-scale models for multiphase flow in porous media. *Proc. Natl Acad. Sci. USA* **116** (28), 13799–13806.

ZHAO, B., PAHLAVAN, A.A., CUETO-FELGUEROSO, L. & JUANES, R. 2018 Forced wetting transition and bubble pinch-off in a capillary tube. *Phys. Rev. Lett.* **120** (8), 084501.

ZOU, S., ARMSTRONG, R.T., ARNS, J.-Y., ARNS, C.H. & HUSSAIN, F. 2018 Experimental and theoretical evidence for increased ganglion dynamics during fractional flow in mixed-wet porous media. *Water Resour. Res.* **54** (5), 3277–3289.